Solar Energy Materials & Solar Cells 117 (2013) 251–258

Contents lists available at SciVerse ScienceDirect

Solar Energy Materials & Solar Cells

journal homepage: www.elsevier.com/locate/solmat

Evaluation of recombination processes using the local ideality factor of carrier lifetime measurements

Ziv Hameiri [a,*], Keith McIntosh [b], GuangQi Xu [c]

[a] Solar Energy Research Institute of Singapore, National University of Singapore, Singapore 117574, Singapore
[b] PV Lighthouse, Coledale, NSW 2515, Australia
[c] The University of New South Wales, Sydney, NSW 2052, Australia

ARTICLE INFO

Article history:
Received 26 February 2013
Accepted 20 May 2013

Keywords:
Effective lifetime
Photoconductance
Photoluminescence
Ideality factor
Silicon wafers
Solar cells

ABSTRACT

The mechanisms that limit the performance of a solar cell can be often identified by an assessment of the solar cell's local ideality factor m. Typically, m is extracted from the current–voltage curve of a completed solar cell and plotted as a function of voltage. In this study, m is extracted from photoluminescence measurements of the effective carrier lifetime and plotted against the excess carrier concentration Δn or the implied open-circuit voltage V_{oci}. It is shown that a plot of $m(\Delta n)$ or $m(V_{oci})$ is a powerful way to analyse recombination processes within a silicon wafer, where its main advantage is that it can be determined from wafers that have neither metal contacts nor a p–n junction. With an $m(\Delta n)$ plot, one can readily identify a range of Δn (or voltage) that is dominated by a single recombination mechanism, or that constitutes a transition from one dominant mechanism to another. One can also identify the dominating recombination mechanisms at a cell's maximum power point. In this paper we demonstrate the application of extracting an $m(\Delta n)$ curve, and we show how it is affected by Shockley–Read–Hall and Auger recombination in the bulk, and by fixed charge in a dielectric coating.

1. Introduction

The mechanisms that limit the performance of a solar cell can be often identified by an assessment of the solar cell's local ideality factor m [1,2]. Typically, m is extracted from the current–voltage curve of a completed solar cell and plotted as a function of voltage [1–4]. In this study, m is extracted from a measurement of the effective carrier lifetime τ_{eff} and plotted against the excess carrier concentration Δn or the implied open-circuit voltage V_{oci} [5]. It is shown that a plot of $m(\Delta n)$ or $m(V_{oci})$ is a powerful contactless method to analyse recombination processes within a silicon wafer.

The local ideality factor can be defined as [1]

$$U \propto (n \times p)^{1/m}, \tag{1}$$

where U is the recombination rate, and n and p are the concentrations of free electrons and holes. The local ideality factor is therefore readily determined by photoconductance (PC) or photoluminescence (PL), which measure U as a function of either $(n+p)$ or $(n \times p)$. Appendix A shows how Eq. (1) relates to the common definition used for completed solar cells, which also incorporates the effects of shunting, series resistance and 2D effects.

By taking the derivative of Eq. (1) with respect to Δn and assuming that (i) the excess electron and hole concentrations are both equal to Δn, and (ii) $\Delta n \gg n_i^2/N$, (where N is the bulk doping concentration and n_i is the intrinsic carrier concentration), m can be expressed as a function of Δn:

$$m = \left(\frac{1}{n} + \frac{1}{p}\right) U \frac{d\Delta n}{dU} = \frac{2\Delta n + N}{\Delta n(\Delta n + N)} U \frac{d\Delta n}{dU}. \tag{2}$$

Note that Eq. (2) holds for wafers only; it is not necessarily accurate for completed solar cells, where m is affected by other effects, such as series resistance, 2D effects etc.

Alternatively, m can be expressed as a function of V_{oci}, which is equivalent to the separation of the quasi-Fermi levels and therefore given by

$$V_{oci} = \frac{kT}{q} \ln\left(\frac{n \times p}{n_i^2}\right), \tag{3}$$

where q is the elementary charge, k Boltzmann's constant and T the absolute temperature [6]. Combining this definition of V_{oci} with Eq. (1) gives

$$m = \frac{q}{kT}\left(\frac{d(\ln(U))}{dV_{oci}}\right)^{-1} = \frac{q}{kT} U \frac{dV_{oci}}{dU}. \tag{4}$$

In this work, our experiments are in steady-state or near steady-state, whereby the generation rate G equals U. Under these conditions, m can be expressed as either:

$$m = \frac{2\Delta n + N}{\Delta n(\Delta n + N)} G \frac{d\Delta n}{dG}, \tag{5}$$

* Corresponding author. Tel.: +65 66011377; fax: +65 67751943.
E-mail address: ziv.hameiri@gmail.com (Z. Hameiri).

0927-0248/$ - see front matter © 2013 Elsevier B.V. All rights reserved.
http://dx.doi.org/10.1016/j.solmat.2013.05.040

or

$$m = \frac{q}{kT}\left(\frac{d(\ln(G))}{dV_{oci}}\right)^{-1} = \frac{q}{kT}G\frac{dV_{oci}}{dG}. \quad (6)$$

Thus, $m(\Delta n)$ and $m(V_{oci})$ can be determined with Eqs. (5) and (6) using either PC or PL-based measurements. The resulting plots provide information that is not immediately apparent from the standard analysis of $\tau_{eff}(\Delta n)$, such as range of Δn that is dominated by a single recombination mechanism, or that constitutes a transition from one dominant mechanism to another.

The main advantage of using PC or PL to determine m is that it can be performed on wafers that do not have metal contacts or even a p–n junction. The local ideality factor is therefore unaffected by the shunting or series resistance related to metal contacts, which frequently prevent an assessment of recombination processes at low and high voltages in solar cells. By studying m before and after the formation of metal contacts, one can evaluate how they influence the dominant recombination mechanisms. One can also assess how the various recombination processes influence the fill factor *FF* of the resulting solar cell.

2. Modelling

A model following the approach of Girisch et al. [7] was developed using the software package Mathematica 8 (Wolfram Research). The inputs of this model are the sample parameters (N and thickness), the surface defect parameters (surface state density D_{it}, capture cross section of electrons σ_n and holes σ_p) and the fixed charge density within the dielectric Q_f. The surface potential ψ_s is determined as a function of Δn assuming charge neutrality [7]. Using ψ_s, the electron and hole concentrations at the surface are calculated. Based on these concentrations, the surface recombination is computed by the Shockley–Read–Hall (SRH) equation [8,9]. More information regarding these calculations can be found in Refs. [7,10].

The bulk recombination rate U_b is determined as the sum of the SRH (using inputs regarding defects in the bulk, such as energy level and the electron and hole lifetime parameters τ_{n0} and τ_{p0}), Auger and radiative [11] recombination terms:

$$U_{bi} = \Sigma U_{b\_i} = U_{b,SRH} + U_{b,Auger} + U_{b,Radiative}, \quad (7)$$

where U_{b_i} represents the different bulk recombination rates. At steady state G is equal to the sum of the different recombination processes and therefore can be expressed as:

$$G = \Sigma U_i = U_s\left(\frac{2}{W}\right) + (U_{b,SRH} + U_{b,Auger} + U_{b,Radiative}), \quad (8)$$

where U_i represents the different recombination mechanisms, U_s is the surface recombination and W is the sample thickness. The simulated m can then be extracted using Eq. (5) or Eq. (6).

3. Experimental

3.1. Sample preparation

Four float-zone (FZ) 1 Ω cm p-type (100) and four Czochralski (Cz) 1.7 Ω cm n-type (100) wafers were used in this study. The wafer thickness after an alkali saw damage etch was 210–220 μm. After a full RCA clean [12] and HF (hydrofluoric) dip, amorphous silicon nitride (SiN_x) was deposited onto both surfaces using a plasma-enhanced chemical vapour deposition (PECVD) system manufactured by Roth & Rau (AK-400). The refractive index and the film thickness were measured by a dual-mode ellipsometer at a single wavelength of 632.8 nm, using a single-side polished wafers, and found to be 2.4 and 75 nm, respectively. The effective lifetime was measured as a function of Δn using a PL-based system under near steady-state conditions and using the generalized analysis [13]. The local ideality factor was then calculated using Eq. (5) or Eq. (6).

Table 1
Effective lifetime and calculated S_{eff_ul} and τ_{b,SRH_ll} at Δn of 1×10^{15} cm^{-3}.

	τ_{eff} [μs]	S_{eff_ul} [cm/s]	τ_{b,SRH_ll} [μs]
p-type (1 Ω cm)	1611	1.1	2800
n-type (1.7 Ω cm)	489	19.2	504

In order to evaluate the passivation quality, the surface recombination velocity S_{eff} was extracted from τ_{eff} at Δn of 1×10^{15} cm^{-3}, using the following relationships:

$$\frac{1}{\tau_{eff}} = \frac{1}{\tau_b} + \frac{1}{\tau_s}, \quad (9)$$

$$\tau_s = \frac{W}{2S_{eff}}, \quad (10)$$

which combined to give

$$S_{eff} = \frac{W}{2}\left(\frac{1}{\tau_{eff}} - \frac{1}{\tau_b}\right), \quad (11)$$

where τ_b is the bulk lifetime and τ_s is the surface lifetime. Note that Eq. (10) can only be used when S_{eff} is relatively small [14]. As the limiting value for the samples presented in this study was calculated to be 470 cm/s, this expression contains negligible error.

The upper limit of S_{eff} (S_{eff_ul}) was calculated using the intrinsic limit [11] on τ_b, while the lower limit of the bulk SRH lifetime τ_{b,SRH_ll} was calculated under the assumption of no surface recombination using:

$$\frac{1}{\tau_{b,SRH\_ll}} = \frac{1}{\tau_{eff}} - \left(\frac{1}{\tau_{b,Auger}} + \frac{1}{\tau_{b,Rad}}\right), \quad (12)$$

where $\tau_{b,Auger}$ and $\tau_{b,Rad}$ are the Auger lifetime and the radiative lifetime, respectively.

Table 1 presents τ_{eff} and the calculated S_{eff_ul} and τ_{b,SRH_ll} at Δn of 1×10^{15} cm^{-3}. The very low S_{eff} obtained for both wafer polarities indicates that τ_{eff} is not dominated by surface recombination in either sample at this Δn. Furthermore, the high τ_{b,SRH_ll} (particularly that of the p-type sample) suggests that the bulk lifetime of these samples is relatively high.

3.2. Measurement system

In order to measure τ_{eff} at very low Δn, a PL-based lifetime system [15] was employed since it is minimally affected by artifacts such as trapping [16–18] and depletion region modulation [19–22].

The PL system is a modified Sinton Consulting WCT-120 instrument [23]. An additional silicon diode ('PL sensor') was integrated to detect the spontaneous emission. The signal is fed into a low-noise preamplifier before being analysed. The illumination source was either a 1.5 W array of 810 nm light emitting diodes (LEDs) or a high-power xenon flash. The control of the light source is accomplished by a digital-analogue port of a data acquisition card. The software allows the user to design a wide range of waveforms, to choose the number of repetitions, the number of data points and the desired signal averaging. More details on the system can be found in Refs. [15,20,24].

4. Results and discussion

4.1. Transition from SRH recombination to Auger recombination

As a starting point, τ_{eff} of a p-type sample was simulated as described above. Bulk recombination was modelled with a single midgap SRH centre and Auger recombination. The surface recombination was made negligible by setting D_{it} to zero. Table 2 summarizes the parameters used in this simulation.

Fig. 1(a) presents the simulated bulk SRH lifetime $\tau_{b,SRH}$, $\tau_{b,Auger}$ and τ_{eff} as a function of Δn (and as a function of V_{oci} on the upper x axis). Consistent with the SRH equation, $\tau_{b,SRH}$ is constant and equal to the minority carrier lifetime at low injection. It then increases at medium injection and approaches the sum of the minority and majority carrier lifetimes at high injection. The Auger lifetime, is also constant at low injection but it decreases rapidly from mid-injection onwards. Combined, the net lifetime τ_{eff} is dominated by SRH recombination at low Δn and by Auger recombination at high Δn, with the transition from SRH to Auger being clearly evident in Fig. 1(a). Such a transition is well documented, see for example Refs. [25,26].

We now examine m as a function of Δn (and V_{oci}), as presented in Fig. 1(b). At low Δn, m is unity, which characterizes all ideal recombination mechanisms at low injection. The local ideality factor then increases at moderate injection and would approach 2 if SRH was to dominate at high injection. But instead, m peaks as the dominant mechanism transition from SRH to Auger recombination, and m then decreases to approach 0.755, which is consistent with the Auger recombination equation at high injection [11,27].

It is worth noting here that while both $\tau_{eff}(\Delta n)$ and $m(\Delta n)$ contain a peak, the peak does not occur at the same Δn; since $m(\Delta n)$ relates to the derivative of $\tau_{eff}(\Delta n)$, the peak in $m(\Delta n)$ corresponds to the inflection point in $\tau_{eff}(\Delta n)$.

Two important voltages of any solar cell are its maximum power point voltage V_{MPP} and open-circuit voltage V_{oc}. Often, there is a transition from one dominant recombination mechanism to another between V_{MPP} and V_{oc}, as would occur in the example of Fig. 1 if it was a typical silicon solar cell. Such transitions cause the FF to deviate from its ideal value. Evaluation of a Suns–V_{oc} curve [28] can quantify how such transitions affect the implied fill factor FF_i of the sample. A complementary assessment of the $m(V_{oci})$ can help to deduce the cause of this transition.

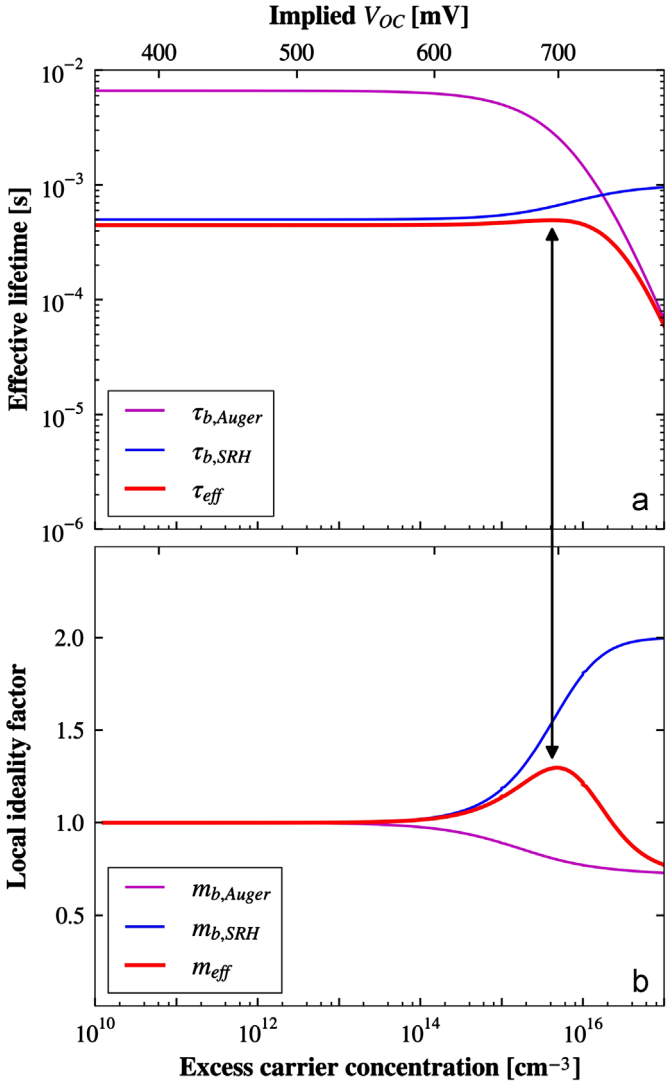

Fig. 1. Simulated effective lifetime as a function of the excess carrier concentration (and implied V_{oc}—upper scale) for a case where the effective lifetime is influenced only by a single SRH recombination centre at the bulk and Auger recombination (a) and the extracted local ideality factor as a function of excess carrier concentration of the same sample (b).

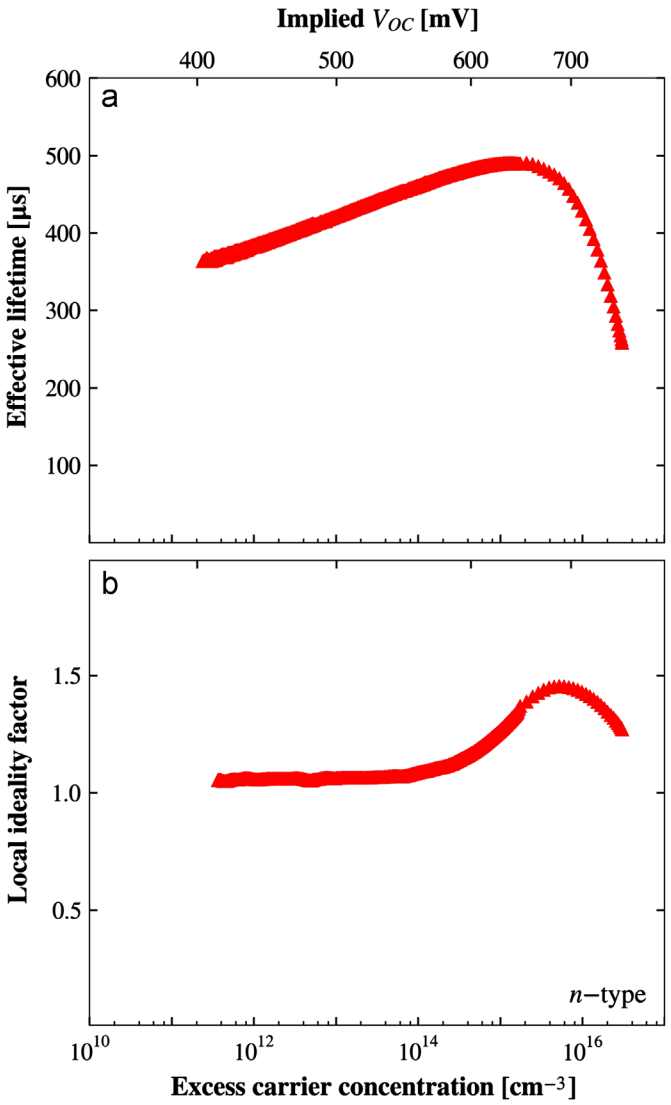

Fig. 2. Measured effective lifetime as a function of the excess carrier concentration (and implied V_{oc}–upper scale) of a representative n-type sample (a) and the extracted local ideality factor as a function of excess carrier concentration of the same sample (b).

A practical example that is similar to the simulated case of Fig. 1 is presented in Fig. 2. This data was measured for an *n*-type substrate that is well passivated by a positively charged dielectric (SiN_x), where the positive charge has only a limited impact on the transition between dominant recombination mechanisms (see more below). Fig. 2(a) presents τ_{eff} as a function of Δn of a representative *n*-type sample (see Section 3.1). Since $S_{eff} < 20$ cm/s, it can be concluded that τ_{eff} of this sample is limited by $\tau_{b,SRH}$ at low and medium Δn and by $\tau_{b,Auger}$ at higher Δn.

Fig. 2(b) plots m of the same sample as a function of Δn. Similar to Fig. 1(b), this curve shows clearly the transition between SRH and Auger recombination. The local ideality factor is constant and close to unity at low Δn, consistent with recombination that is dominated by a single ideal SRH defect. It then increases as the dominant SRH recombination shifts from low to high injection. These features are not immediately evident from the $\tau_{eff}(\Delta n)$ curve. Finally, at $\Delta n > 3 \times 10^{15}$ cm^{-3}, m peaks and declines as the dominant recombination mechanism transitions from the SRH defect to Auger recombination.

If this recombination occurred in a typical silicon solar cell, then the transition from being dominated by low-injection SRH to high-injection SRH would occur in a voltage range between V_{MPP} and V_{oc} (530–640 mV). Consequently, the solar cell's *FF* would be lower than ideal. While plot of Suns–V_{oc} would quantify this reduction, the ultimate cause would be more apparent in the $m(\Delta n)$ plot.

4.2. Influence of surface recombination

The influence of a high surface recombination is now described with the examples of Fig. 3. Firstly, and without surface charge, Fig. 3(a) and (b) present a similar example to Fig. 1 except that τ_s was chosen to be the limiting factor by setting a much higher D_{it} (see Table 2). In this simulation $\tau_{b,SRH}$ is sufficiently higher than τ_s that it does not impact τ_{eff}. Although τ_{eff} in Fig. 3 is significantly lower than in Fig. 1, m is similar since in both cases the dominant recombination mechanism transitions from SRH to Auger at mid-to-high injection. Again, it is worth noting that the peaks in $\tau_{eff}(\Delta n)$ and $m(\Delta n)$ do not occur at the same Δn.

The influence of fixed surface charge is introduced with Fig. 3 (c) and (d). As listed in Table 2, the simulation now includes a large and positive fixed charge, while the rest of the parameters are unchanged. The red curves, which plot $\tau_{eff}(\Delta n)$ and $m(\Delta n)$ is now considerably different to the previous examples; in fact, $m(\Delta n)$ now contains two peaks!

The peak in $m(\Delta n)$ at high Δn is caused by the transition from low-injection SRH to high-injection SRH to Auger recombination in the same manner as Figs. 1(b) and 3(b). The large peak at low Δn occurs over the range of carrier concentrations dominated by surface recombination and is influenced by the injection dependence of S_{eff} introduced by field effect passivation. Notice that although the first peak in the $m(\Delta n)$ curve is clearly evident, the corresponding feature in the $\tau_{eff}(\Delta n)$ curve is barely noticeable.

Specifically, the peak at low injection is caused as follows. At low Δn, the positive charge increases the electron surface concentration n_s, making it higher than the hole surface concentration p_s (i.e., weak inversion—see Appendix B). As n_s and p_s are similar under this condition, the recombination rate at the surface is enhanced. However, at higher Δn, the fixed positive charge invokes a stronger inversion layer in the moderately doped *p*-type substrate ($N_A = 1 \times 10^{16}$ cm^{-3}). In this layer the holes and not the electrons are the minority carriers. Due to low hole concentration in this layer, the ratio n_s/p_s increases and the recombination processes are significantly slowed, hence τ_{eff} is improved compared to a sample without fixed charge [such as the sample of Fig. 3(a)]. This transition is very clear in the $m(\Delta n)$ plot. The peak at Δn of 1×10^{11} cm^{-3} indicates a variation of the surface recombination [29] and correspond to the aforementioned transition from surface recombination limited by electrons (at low Δn) to recombination limited by holes (at higher Δn).

Fig. 4(a) presents the measured τ_{eff} of a representative *p*-type sample passivated with SiN_x (see Section 3.1). Note the wide range

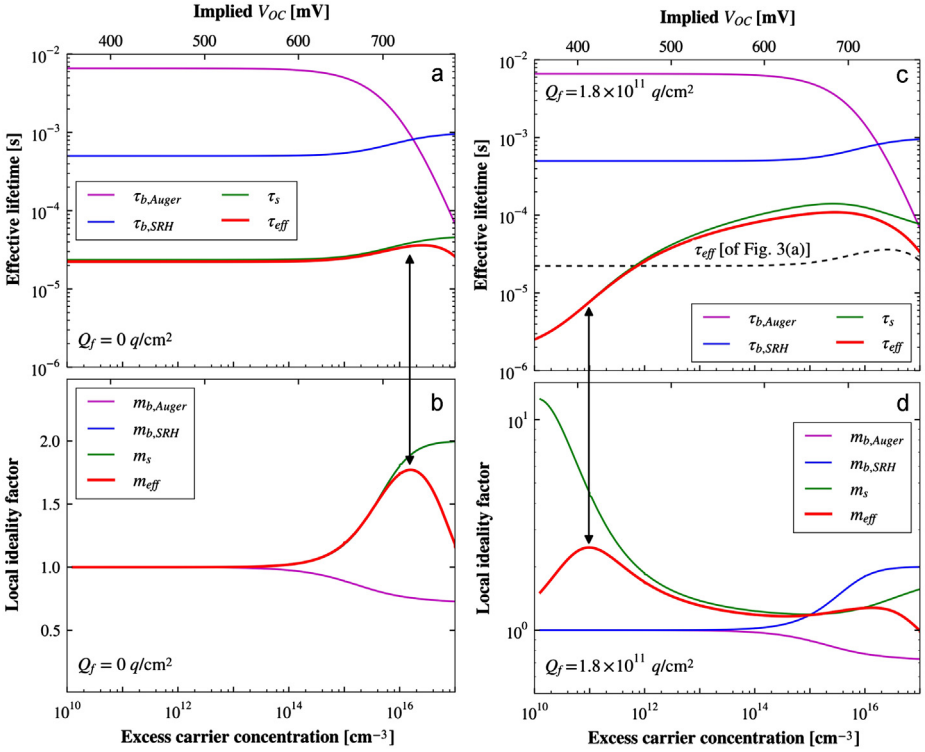

Fig. 3. Simulated effective lifetime as a function of the excess carrier concentration (a, c) and the extracted local ideality factor as a function of excess carrier concentration (b, d). In (a, b) the surface recombination is simulated using only D_{it} (Q_f was set to zero), while in (c, d) surface recombination is modelled using both D_{it} and Q_f (see Table 2).

of Δn (from 1×10^{10} to 5×10^{16} cm^{-3}) provided by the PL-based system, which significantly extends the range obtained by the PC-based system.

The observed dependence of τ_{eff} on Δn accords with the simulation results [see Fig. 3(c)] and the findings of other researchers [30–32]. At high Δn, τ_{eff} is limited by Auger recombination, while at low Δn it is primarily influenced by the injection level dependence of S_{eff}. This dependence is influenced not only by the mentioned field effect, created by the positive fixed charge within the SiN_x film [33,34], but also by the asymmetry in the capture cross section of electrons and holes. This large asymmetry ($\sigma_n/\sigma_p=10^1$–10^6 at midgap [34,35]) is predicted to result in a strong injection level dependence due to a transition whereby the recombination switches from being limited by the capture of electrons to the capture of holes [36]. A significant decrease in S_{eff} is expected once the injection level exceeds a critical value of $n_s/p_s\approx\sigma_p/\sigma_n$ [37,38].

This transition from electron-limited to hole-limited surface recombination is clearly shown in Fig. 4(b), which presents m as a function of Δn. Similar to Fig. 3(d), the noticeable peak at Δn of 7×10^{10} cm^{-3} indicates a transition between different limiting processes. At low injection the surface recombination is limited by the minority carriers (electrons) concentration, while at higher injection level majority carrier (holes) concentration is the limiting element.

Similar to the n-type sample (Fig. 2), the FF of a solar cell made on this substrate would be affected by the transition between SRH at low and high injections, as this transition happens in the voltage range between V_{MPP} and V_{oc}. Influence of the recombination processes on the FF was also reported by others [39,40].

Comparison between m of the p-type [Fig. 4(b)] and n-type [Fig. 2(b)] substrates is informative. As mentioned before, the peak in $m(\Delta n)$ curve at low injection level is due to the transition from electron-limited to hole-limited surface recombination. However, when using an n-type substrate, the surface recombination is limited only by the hole lifetime (as the electrons' lifetime is significantly lower than that of the holes and due to the fact that no inversion layer is formed by the positive interface charge). As there is no transition between limiting processes when using a positive fixed charge on an n-type substrate, m behaves similarly to Fig. 1(b). The peak at high Δn is due to a transition from low-injection SRH to high-injection SRH to Auger recombination. Due to the relatively low background doping of the n-type 1.7 Ω cm substrate ($N_D=2.8\times10^{15}$ cm^{-3}), this effect starts to dominate at a lower Δn than in the p-type 1 Ω cm substrate.

Table 2
Parameters used for the simulations of Figs. 1 and 3.

Parameter	Fig. 1	Fig. 3(a, b)	Fig. 3(c, d)
N [cm^{-3}]	1×10^{16}	1×10^{16}	1×10^{16}
D_{it} [cm^{-2} eV^{-1}]	0	6×10^{11}	6×10^{11}
σ_n/σ_p	N.A.	1	1
Q_f [q/cm^2]	0	0	$+1.8\times10^{11}$

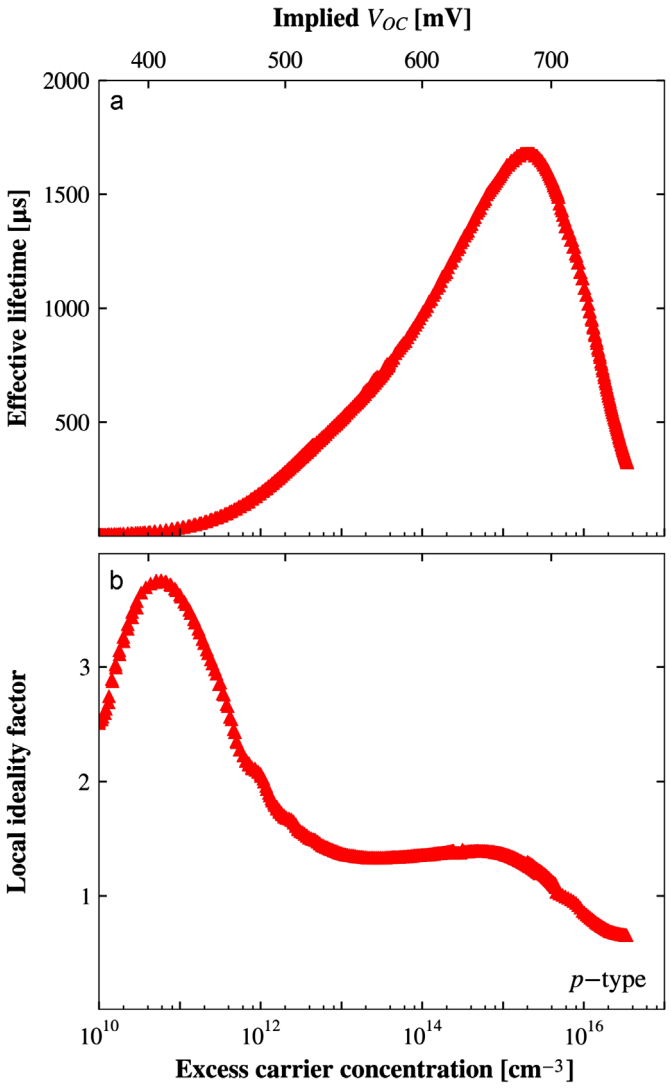

Fig. 4. Measured effective lifetime as a function of the excess carrier concentration (and implied V_{oc}—upper scale) of a representative p-type sample (a) and the extracted local ideality factor as a function of excess carrier concentration of the same sample (b).

4.3. Influence of bulk doping density and fixed charge on the transition voltage

In this section the impact of N and Q_f on the transition range (i.e., the range of V_{oci} or Δn over which the transition occurs) is studied using the model of Section 2. The modelled parameters are summarized in Table 3.

Fig. 5(a) presents the impact of a positive Q_f on m of an n-type substrate. For these simulations, N_D of 3×10^{15} cm^{-3} was used and all other parameters were kept identical. As can be clearly seen, m is independent of Q_f as all the simulated Q_f introduce an accumulation layer beneath the surface. Under this condition, no transition from electron-limited to hole-limited surface recombination occurs. Hence, the only noticed peak is at high Δn due to the transition from SRH to Auger.

Fig. 5(b) presents the influence of N_D on m. Similar to Fig. 5(a), no peak is observed at low and medium Δn. The peak observed at $\Delta n>1\times10^{14}$ cm^{-3} is due to the SRH–Auger transition. Both the starting point of this peak as well as its peak value are influenced by N_D because N_D dictates the Δn range over which SRH

Table 3
Parameters used for the simulations of Fig. 5.

Parameter	Fig. 5(a)	Fig. 5(b)	Fig. 5(c)	Fig. 5(d)
N [cm^{-3}]	3×10^{15}	Vary	1×10^{16}	Vary
D_{it} [cm^{-2} eV^{-1}]	6×10^{11}	6×10^{11}	6×10^{11}	6×10^{11}
σ_n/σ_p	1×10^{4}	1×10^{4}	1×10^{4}	1×10^{4}
Q_f [q/cm^2]	Vary	$+1.2\times10^{11}$	Vary	$+1.2\times10^{11}$

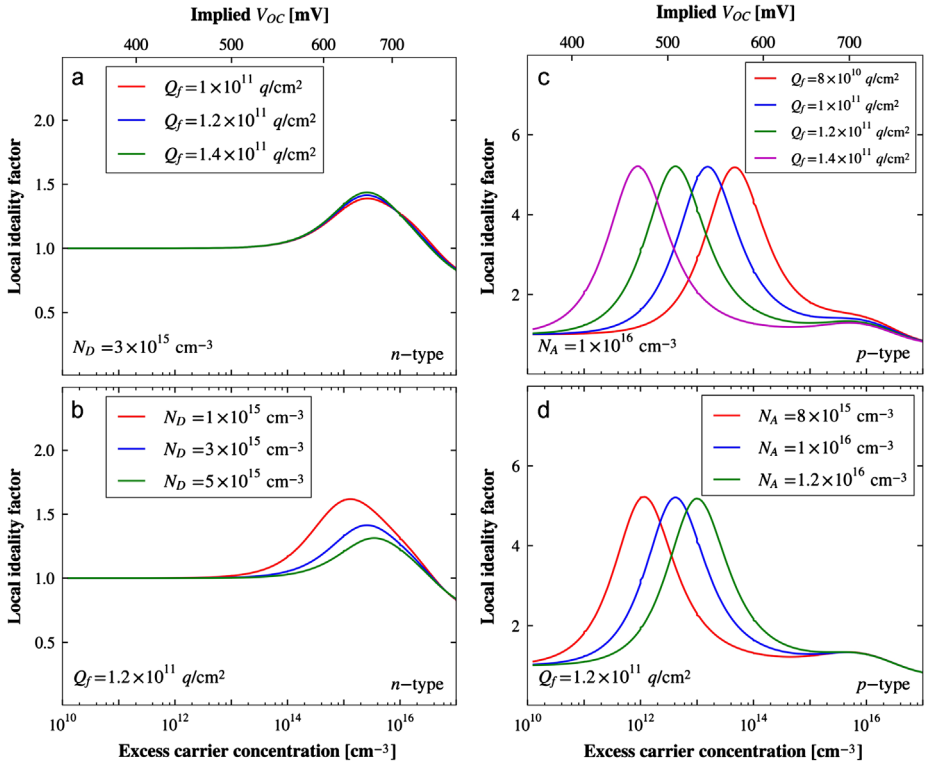

Fig. 5. Simulated local ideality factor as a function of excess carrier concentration of different fixed positive charge densities within the dielectric layer [(a) *n*-type and (c) *p*-type] and for different bulk doping densities [(b) *n*-type and (d) *p*-type].

recombination transitions from low to high injection and m increases from 1 to 2.

Fig. 5(c) shows the impact of a positive Q_f on m, this time for a *p*-type substrate. As can be seen, an increase in charge shifts the peak to lower Δn. A higher Q_f attracts more electrons to the surface and therefore enhances the development of an inversion layer beneath the silicon-dielectric interface (see Appendix B, Fig. B2). Hence, a higher Q_f is beneficial, not only to reduce S_{eff} (by reducing p_s), but also to shift the transition range to voltages below V_{MPP}. The peak at higher Δn ($>10^{15}$ cm^{-3}) can be observed for some of the samples. The formation of this peak requires a transition of SRH recombination from low to high injection before the transition from SRH to Auger starts. The peak is less pronounced for samples whose dominant recombination mechanism switches from SRH to Auger when m is higher than 2 (i.e. for cases where the transition from SRH to Auger starts before the first transition has been ended).

Fig. 5(d) presents $m(\Delta n)$ for a variety of N_A. An increase in N_A shifts the lower peak to higher Δn, as the transition point between depletion and inversion conditions is shifted to higher Δn (see Fig. B3). A higher concentration of electrons (minority carriers) is needed to form an inversion layer when N_A is higher.

5. Conclusions

A contactless method to evaluate recombination processes within silicon wafers, based on m extracted from PC or PL measurements of the effective lifetime, was presented. The resulting $m(\Delta n)$ and $m(V_{oci})$ plots provide information that is not immediately apparent from the standard analysis of $\tau_{eff}(\Delta n)$, such as range of Δn that is dominated by a single recombination mechanism, or that constitutes a transition from one dominant mechanism to another.

The main advantage of using PC or PL to determine m is that they can be performed on wafers that do not have metal contacts or even a *p*–*n* junction. The local ideality factor is therefore unaffected by the shunting or series resistance related to metal contacts, which frequently prevent an assessment of recombination processes at low and high voltages in solar cells. By studying m before and after the formation of metal contacts, one can evaluate how they influence the dominant recombination mechanisms. One can also assess how the various recombination processes influence the *FF* of the resulting solar cell.

Future work will focus on the expansion of the proposed analysis to be used to determine the density of fixed charge in dielectric layers and the capture cross sections of the dominant interface defects.

Acknowledgement

The Solar Energy Research Institute of Singapore (SERIS) is sponsored by the National University of Singapore (NUS) and the Singapore's National Research Foundation (NRF) through the Singapore Economic Development Board (EDB). The funding for this research was received under NRF, Grant NRF-2011EWT-CERP001-015.

Appendix A. On the definition of the local ideality factor

For a solar cell, m is determined from its current–voltage relationship (I–V) [1]:

$$I \propto \exp\left(\frac{q}{kT}\frac{V}{m}\right). \tag{A1}$$

If V were constant at all parts of the cell and equal to V_{oci}, that is, assuming that the cell is not affected by 2D variations or series

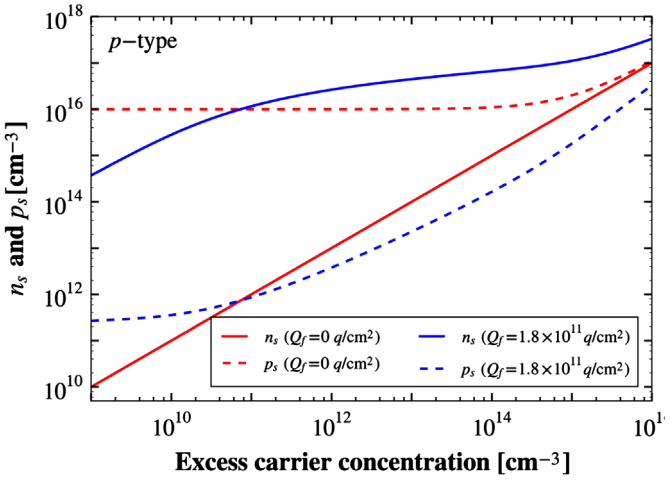

Fig. B1. Electron and hole surface concentration as a function of excess carrier concentration with dielectric charge (blue lines) and without dielectric charge (red lines).

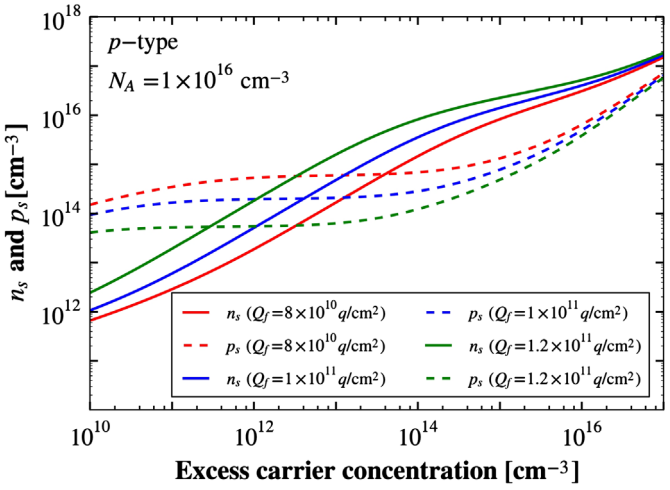

Fig. B2. Electron and hole surface concentration as a function of excess carrier concentration of different dielectric charges.

resistance, then

$$I \propto \exp\left(\frac{q}{kT}\frac{V_{oc\,i}}{m}\right) = \left(\frac{n \times p}{n_i^2}\right)^{1/m} \tag{A2}$$

where Eq. (A2) makes use of Eq. (3).

Under the conditions where I is proportional to U, such as negligible shunt resistance, Eq. (A2) can be written as:

$$U \propto (n \times p)^{1/m} \tag{A3}$$

as written in Eq. (1).

Appendix B. Surface concentrations

Fig. B1 presents n_s and p_s as a function of Δn for the cases where Q_f is zero [Fig. 3(a) and (b)] and where $Q_f = 1.8 \times 10^{11}$ q/cm^2 [Fig. 3 (c) and (d)]. As clearly seen, for $\Delta n < 8 \times 10^{11}$ cm^{-3} the ratio n_s/p_s of the second case is smaller than the ratio p_s/n_s of the first case, resulting with an enhanced surface recombination. However, at $\Delta n > 8 \times 10^{11}$ cm^{-3} an opposite relationship is observed. Note that for the second case, the layer beneath the surface is under an inversion for the entire Δn range.

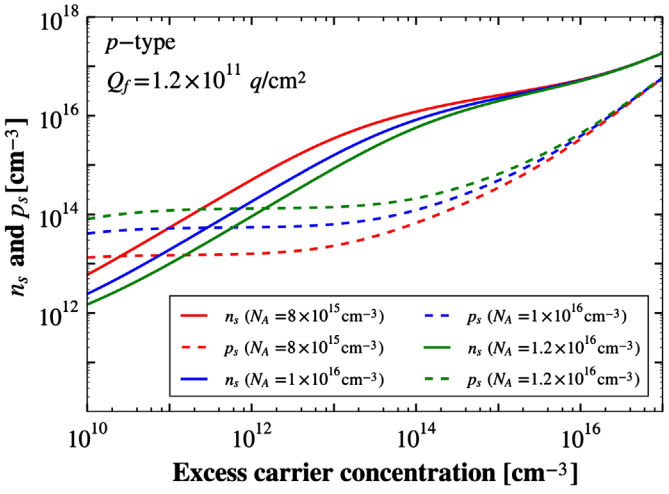

Fig. B3. Electron and hole surface concentration as a function of excess carrier concentration of different bulk doping densities.

Fig. B2 shows n_s and p_s of Fig. 5(c) as a function of Δn. The transition point between depletion and inversion is shifted to lower Δn, when Q_f is increased.

The surface carrier concentrations n_s and p_s of Fig. 5(d) are presented in Fig. B3 as a function of Δn. The transition point between depletion and inversion is shifted to higher Δn, when N_A is increased.

References

[1] K.R. McIntosh, Lumps, Humps and Bumps: Three Detrimental Effects in the Current–Voltage Curve of Silicon Solar Cells, University of New South Wales, Sydney, Australia, 2001.
[2] S.J. Robinson, G.F. Zheng, R. Bergmann, W. Zhang, Z. Shi, M.A. Green, Opto-electronic characterization of thin-film crystalline silicon solar cells grown from metal solutions, in: Proceedings of the 12th European Photovoltaic Solar Energy Conference, 1994, pp. 1831–1834.
[3] Z. Hameiri, L. Mai, S.R. Wenham, Advantages of photoplating for laser doped solar cells, Progress in Photovoltaics: Research and Applications 19 (2011) 511–516.
[4] D. Kray, K.R. McIntosh, Analysis of selective phosphorous laser doping in high-efficiency solar cells, IEEE Transactions on Electron Devices 56 (2009) 1645–1650.
[5] R. Sinton, A. Cuevas, Contactless determination of current–voltage characteristics and minority-carrier lifetimes in semiconductors from quasi-steady-state photoconductance data, Applied Physics Letters 69 (1996) 2510–2512.
[6] R.A. Sinton, A. Cuevas, A quasi-steady state open-circuit voltage method for solar cell characterization, in: Proceedings of the 16th European Photovoltaic Solar Energy Conference, Glasgow, UK, 2000, pp. 1152–1155.
[7] R.B.M. Girisch, R.P. Mertens, R.F. De Keersmaecker, Determination of Si–SiO$_2$ interface recombination parameters using a gate-controlled point-junction diode under illumination, IEEE Transactions on Electron Devices 35 (1988) 203–222.
[8] W. Shockley, W.T. Read, Statistics of the recombinations of holes and electrons, Physical Review 87 (1952) 835–842.
[9] R.N. Hall, Electron–hole recombination in germanium, Physical Review 87 (1952) 387.
[10] A. Aberle, S. Glunz, W. Warta, Impact of illumination level and oxide parameters on Shockley-Read-Hall recombination at the Si–SiO$_2$ interface, Journal of Applied Physics 71 (1992) 4422–4431.
[11] M. Kerr, A. Cuevas, General parameterization of Auger recombination in crystalline silicon, Journal of Applied Physics 91 (2002) 2473–2480.
[12] W. Kern, The evolution of silicon wafer cleaning technology, Journal of the Electrochemical Society 137 (1990) 1887–1892.
[13] H. Nagel, C. Berge, A. Aberle, Generalized analysis of quasi-steady-state and quasi-transient measurements of carrier lifetimes in semiconductors, Journal of Applied Physics 86 (1999) 6218–6221.
[14] A.B. Sproul, Dimensionless solution of the equation describing the effect of surface recombination on carrier decay in semiconductors, Journal of Applied Physics 76 (1994) 2851–2854.
[15] T. Trupke, R.A. Bardos, Photoluminescence: a surprisingly sensitive lifetime technique, in: Proceedings of the 31st IEEE Photovoltaic Specialists Conference, 2005, pp. 903–906.
[16] D. Macdonald, A. Cuevas, Trapping of minority carriers in multicrystalline silicon, Applied Physics Letters 74 (1999) 1710–1712.

[17] R.A. Bardos, T. Trupke, M.C. Schubert, T. Roth, Trapping artifacts in quasi-steady-state photoluminescence and photoconductance lifetime measurements on silicon wafers, Applied Physics Letters 88 (2006) 053504–053513.
[18] K. McIntosh, A model for the steady-state photoconductance of an abrupt p-n junction semiconductor diode assuming flat quasi-fermi levels, IEEE Transactions on Electron Devices 54 (2007) 346–353.
[19] P. Cousins, D. Neuhaus, J. Cotter, Experimental verification of the effect of depletion-region modulation on photoconductance lifetime measurements, Journal of Applied Physics 95 (2004) 1854–1858.
[20] T. Trupke, R.A. Bardos, F. Hudert, P. Wurfel, J. Zhao, A. Wang, M.A. Green, Effective excess carrier lifetimes exceeding 100 milliseconds in float zone silicon determined from photoluminescence, in: Proceedings of the 19th European Photovoltaic Solar Energy Conference, Paris, 2004, pp. 758–761.
[21] K. McIntosh, B. Paudyal, D. Macdonald, Generalized procedure to determine the dependence of steady-state photoconductance lifetime on the occupation of multiple defects, Journal of Applied Physics 104 (2008) 084503–084506.
[22] K. McIntosh, B. Paudyal, D. Macdonald, Erratum: generalized procedure to determine the dependence of steady-state photoconductance lifetime on the occupation of multiple defects, Journal of Applied Physics 104 (2008) 084503. K. McIntosh, B. Paudyal, D. Macdonald, Journal of Applied Physics 106 (2009) 029901–029902.
[23] R. Sinton, D. Macdonald, WCT-120 Photoconductance Lifetime Tester: User Manual, publisher:Sinton Instruments. Inc., 2006.
[24] Z. Hameiri, K. McIntosh, T. Trupke, Uncertainty in photoluminescence-based effective minority carrier lifetime measurements, in: Proceedings of the 38th IEEE Photovoltaic Specialists Conference (PVSC), 2012.
[25] A. Richter, S. Glunz, F. Werner, J. Schmidt, A. Cuevas, Improved quantitative description of Auger recombination in crystalline silicon, Physical Review B 86 (2012) 165202–165214.
[26] Y. Wan, K. McIntosh, A. Thomson, A. Cuevas, Immeasurably low surface recombination velocity passivated by low absorption silicon nitride on c-Si, in: Proceedings of the 38th IEEE Photovoltaic Specialists Conference (PVSC), 2012.
[27] M.A. Green, Silicon Solar Cells: Advanced Principles and Practice, University of New South Wales, Sydney, Australia, 1995.
[28] A. Cuevas, R.A. Sinton, Prediction of the open-circuit voltage of solar cells from the steady-state photoconductance, Progress in Photovoltaics: Research and Applications 5 (1997) 79–90.
[29] M. Bail, M. Schulz, R. Brendel, Space-charge region-dominated steady-state photoconductance in low-lifetime Si wafers, Applied Physics Letters 82 (2003) 757–759.
[30] M.J. Kerr, A. Cuevas, Recombination at the interface between silicon and stoichiometric plasma silicon nitride, Semiconductor Science and Technology 17 (2002) 166–172.
[31] A. Cuevas, M.J. Kerr, J. Schmidt, Passivation of crystalline silicon using silicon nitride, in: Proceedings of the 3rd World Conference on Photovoltaic Energy Conversion, 2003, pp. 913–918.
[32] A. Aberle, T. Lauinger, J. Schmidt, R. Hezel, Injection-level dependent surface recombination velocities at the silicon-plasma silicon nitride interface, Applied Physics Letters 66 (1995) 2828–2830.
[33] S. Dauwe, J. Schmidt, A. Metz, R. Hezel, Fixed charge density in silicon nitride films on crystalline silicon surfaces under illumination, in: Proceedings of the 29th IEEE Photovoltaic Specialists Conference, 2002, pp. 162–165.
[34] A.G. Aberle, Crystalline Silicon Solar Cells: Advanced Surface Passivation and Analysis, University of New South Wales, Sydney, Australia, 2004.
[35] J. Schmidt, F. Schuurmans, W. Sinke, S. Glunz, A. Aberle, Observation of multiple defect states at silicon–silicon nitride interfaces fabricated by low-frequency plasma-enhanced chemical vapour deposition, Applied Physics Letters 71 (1997) 252–254.
[36] A. Aberle, S. Robinson, A. Wang, J. Zhao, S. Wenham, M. Green, High-efficiency silicon solar cells: fill factor limitations and non-ideal diode behaviour due to voltage-dependent rear surface recombination velocity, Progress in Photovoltaics: Research and Applications 1 (1993) 133–143.
[37] A. Aberle, S. Glunz, W. Warta, Field effect passivation of high efficiency silicon solar cells, Solar Energy Materials and Solar Cells 29 (1993) 175–182.
[38] E. Yablonovitch, R.M. Swanson, W.D. Eades, B.R. Weinberger, Electron–hole recombination at the Si–SiO_2 interface, Applied Physics Letters 48 (1986) 245–247.
[39] J. Schmidt, A. Cuevas, S. Rein, S. Glunz, Fill factor limitations and non-ideal diode behaviour of Czochralski silicon solar cells due to light-induced recombination centres, in: Proceedings of the 17th European Photovoltaic Solar Energy Conference, 2001, pp. 1396–1399.
[40] D. Macdonald, A. Cuevas, Reduced fill factors in multicrystalline silicon solar cells due to injection-level dependent bulk recombination lifetimes, Progress in Photovoltaics: Research and Applications 8 (2000) 363–375.